PNAS RESEARCH ARTICLE | APPLIED BIOLOGICAL SCIENCES CHEMISTRY OPEN ACCESS

Precision treatment of viral pneumonia through macrophage-targeted lipid nanoparticle delivery

Gan Zhao[a,b,c,1], Lulu Xue[d,1], Hannah C. Geisler[d], Junchao Xu[d], Xinyuan Li[a,b,c], Michael J. Mitchell[b,d,e,f,g,h,2], and Andrew E. Vaughan[a,b,c,2]

Edited by Daniel J. Siegwart, The University of Texas Southwestern Medical Center, Dallas, TX; received August 25, 2023; accepted January 5, 2024 by Editorial Board Member Carl F. Nathan

Macrophages are integral components of the innate immune system, playing a dual role in host defense during infection and pathophysiological states. Macrophages contribute to immune responses and aid in combatting various infections, yet their production of abundant proinflammatory cytokines can lead to uncontrolled inflammation and worsened tissue damage. Therefore, reducing macrophage-derived proinflammatory cytokine release represents a promising approach for treating various acute and chronic inflammatory disorders. However, limited macrophage-specific delivery vehicles have hindered the development of macrophage-targeted therapies. In this study, we screened a pool of 112 lipid nanoparticles (LNPs) to identify an optimal LNP formulation for efficient siRNA delivery. Subsequently, by conjugating the macrophage-specific antibody F4/80 to the LNP surface, we constructed MacLNP, an enhanced LNP formulation designed for targeted macrophage delivery. In both in vitro and in vivo experiments, MacLNP demonstrated a significant enhancement in targeting macrophages. Specifically, delivery of siRNA targeting TAK1, a critical kinase upstream of multiple inflammatory pathways, effectively suppressed the phosphorylation/activation of NF-kB. LNP-mediated inhibition of NF-kB, a key upstream regulator in the classic inflammatory signaling pathway, in the murine macrophage cell line RAW264.7 significantly reduced the release of proinflammatory cytokines after stimulation with the viral RNA mimic Poly(I:C). Finally, intranasal administration of MacLNP-encapsulated TAK1 siRNA markedly ameliorated lung injury induced by influenza infection. In conclusion, our findings validate the potential of targeted macrophage interventions in attenuating inflammatory responses, reinforcing the potential of LNP-mediated macrophage targeting to treat pulmonary inflammatory disorders.

lipid nanoparticles | inhalation delivery | nanomedicine | RNAi therapeutics | pneumonia

Significance

Tissue- or cell-specific delivery within the body is currently one of the most critical challenges in the field of nanodelivery. Our work demonstrates that an antibody-conjugated lipid nanoparticle strategy, when administered intranasally, effectively targets lung macrophages, an essential immune cell type involved in numerous disease states as well as in proper tissue homeostasis. Further, we demonstrate that delivery of siRNA targeting TAK1, an important kinase upstream of inflammatory signaling pathways, can significantly attenuate the proinflammatory macrophage phenotype both in vitro and in vivo. We believe that this work bears high translational relevance given the ongoing COVID-19 epidemic and considering unmet need for better treatments for patients suffering from additional respiratory viral infections including influenza and RSV.

Macrophages, pivotal immune cells in the lung, stand as the foremost guardians of the respiratory system. Their ability to sense and engulf pathogens, release cytokines, and participate in tissue restoration underscores their vital role as a first responder of the innate immune system (1, 2). However, accumulating evidence also points to macrophages as contributors to tissue inflammation and damage. Given that they are a major source of proinflammatory cytokines, they have been implicated in driving the pathology of various diseases including atherosclerosis (3), COVID-19 (4), and desquamative interstitial pneumonia (DIP) (5). Since the inflammatory response driven by macrophages intricately impacts disease progression, exploration of strategies to temper or regulate excessive macrophage-induced inflammation emerges as a promising avenue for the treatment of inflammatory diseases.

Strategies to target macrophages have garnered significant attention, especially with the application of nanomaterials to modulate macrophage function. Numerous studies have demonstrated that nanoparticles significantly enhance the pharmacokinetic properties and chemical stability of loaded therapeutic agents, including small-molecule drugs, peptides, proteins, small interfering RNA (siRNA), and microRNAs (miRNA) (6–8). Nanoparticle delivery strategies targeting inflammatory macrophages have been used successfully in various murine disease models (3, 9–11). Despite the development of diverse nanoparticle delivery methods targeting the mouse lungs (12–15), research into therapeutic strategies specifically focused on lung macrophages remains limited.

Using RNA interference (RNAi) for therapy holds promise in improving disease outcomes (16–19) and holds an advantage over CRISPR/Cas9 for some application in that modulation of gene expression is inherently transient. However, obstacles hinder the widespread application of RNAi therapeutics, specifically concerning efficiently delivering oligonucleotides to target cells while minimizing delivery to nontarget cells. Here, we identified the most effective lipid nanoparticle (LNP) delivery formulation from a pool

Author contributions: G.Z., L.X., M.J.M., and A.E.V. designed research; G.Z., L.X., H.C.G., J.X., and X.L. performed research; G.Z. and L.X. contributed new reagents/analytic tools; G.Z. and L.X. analyzed data; and G.Z., L.X., M.J.M., and A.E.V. wrote the paper.

Competing interest statement: A.E.V., M.J.M., G.Z., and L.X. have filed a patent application based on this study. The other authors declare no competing interest.

This article is a PNAS Direct Submission. D.J.S. is a guest editor invited by the Editorial Board.

[1]G.Z. and L.X. contributed equally to this work.

[2]To whom correspondence may be addressed. Email: mjmitch@seas.upenn.edu or andrewva@vet.upenn.edu.

This article contains supporting information online at https://www.pnas.org/lookup/suppl/doi:10.1073/pnas.2314747121/-/DCSupplemental.

Published February 5, 2024.

of 112 formulations. Following this, we conjugated the F4/80 antibody, a canonical and widely utilized macrophage surface marker, to the LNPs, leading to the successful creation of an advanced LNP we term "MacLNP." This strategy substantially enhances the delivery efficiency to targeted macrophages. Considering relevant target molecules important in macrophage function, TGF-β-activated kinase 1 (TAK1, also referred to as MAP3K7) is a member of the mitogen-activated protein kinase kinase kinase (MAP3K) family. TAK1 regulates multiple downstream pathways including the nuclear factor-κB, c-Jun N-terminal kinase (JNK), p38, and TGF-β signaling pathways, playing a vital role in the fibrotic and inflammatory responses (20). Targeting TAK1 has displayed promising results in mitigating inflammation and fibrosis in experimental pneumoconiosis (21). We therefore employed MacLNP to deliver siRNA targeting TAK1 in influenza-induced pneumonia as a proof-of-concept approach, significantly attenuating local lung inflammation and promoting lung regeneration and repair. This research provides valuable insights targeting macrophages for the treatment of lung inflammatory diseases.

Results

Design of LNP Formulations. Branched ionizable lipids (lipidoids) are beneficial for potent RNA delivery in various applications, including vaccination, RNAi therapeutics, protein replacement therapy, gene editing, and cancer therapy (8, 22–25). Notably, SM-102 lipid, a key component in one of the highly effective FDA-approved COVID-19 vaccines, employs a branched tail structure for mRNA delivery, underscoring the significance of such branched architectures (8). The branched configuration introduces a larger chemical space, thereby increasing the distance between tails to form a more cone-shaped ion pair with the anionic membrane phospholipid, facilitating efficient endosome disruption (22, 23, 25). Consequently, this enhanced fusogenicity is pivotal for achieving effective delivery. While branched tail structures have been widely employed (22, 23, 25), the degree of branching tails as a discrete variable that influences genetic cargo delivery has not been thoroughly investigated in previous studies (22, 23, 25). In this study, we employ a classic esterification reaction to synthesize branched tails with various branching degrees (Fig. 1 *A*–*C* and *SI Appendix*, Figs. S1–S4), then coupling these tails into various amine cores to create a library of branched lipidoids through Michael- addition reaction (Fig. 1*C* and *SI Appendix*, Figs. S5 and S6). The 28 generated branched lipidoids were denoted as X-O10b-y, where "X" represents the order of amine heads in this study, "O10b" indicates the ester-based branching tail (10 means the tail length), and "y" indicates the branching degree of alkyl tails.

High-throughput In Vitro Screening of LNP Formulations for Optimal siRNA Delivery Efficiency. To investigate the structure–activity relationship (SAR) of branched lipidoids for siRNA delivery under various classic formulation parameters, 28 different branched lipidoids, 2 different phospholipids (DOPE and DSPC), cholesterol, and 2 different lipid-anchored PEG (C14PEG2K and DMG-PEG2K) were orthogonally used to formulate 112 total branched LNPs encapsulating GFP siRNA (siGFP), which we then used to evaluate in vitro GFP silencing in HepG2-GFP fibroblast cell line (Fig. 2*A*). Branched LNPs were formulated with an ethanol phase containing branched lipidoid, phospholipid, cholesterol, and lipid-anchored poly(ethylene glycol) with a molar ratio of 35:16:46.5:2.5 and an aqueous containing siGFP via pipette mixing (26, 27) (Figs. 1*A* and 2*A*). The resulting branched LNPs exhibited a diverse range of hydrodynamic sizes (100 to 240 nm) (*SI Appendix*, Tables S1 and S2) with monodisperse populations indicated by a polydispersity index (PDI) lower than 0.2 for ~80% of LNPs (*SI Appendix*, Tables S1 and S2), suitable surface charge (*SI Appendix*, Tables S1 and S2), and favorable siRNA encapsulation efficiencies for DOPE based formulations (~84% of them are greater than 70%, *SI Appendix*, Tables S1 and S2), but lower encapsulation capability for DSPC incorporated formulations (*SI Appendix*, Tables S1 and S2). Importantly, all branched LNPs exhibited low cytotoxicity, evidenced by >80% cell viability after LNP transfection (*SI Appendix*, Fig. S7). Moreover, cryo-transmission electron microscopy (cryo-TEM) revealed that representative branched LNP formulated by microfluidic mixing possessed uniform solid core morphology with a diameter smaller than 100 nm for intracellular delivery (Fig. 2 *B* and *C*).

Following in vitro screening in HepG2-GFP cells, we generated heat maps representing the SAR of branched lipidoids formulated under the various parameters that influenced siRNA delivery activity (Fig. 2 *D*–*G* and *SI Appendix*, Fig. S8). A relative hit rate, defined by a GFP silencing efficacy >50%, was used to evaluate the most crucial structural properties influencing siRNA delivery in vitro after treating cells with each branched LNP at siRNA concentrations of 50 nM under the different formulation parameters. Branched lipidoids with four tertiary amines per lipidoid exhibited the highest efficacy, with a hit rate of ~38% across these formulations, likely due to 1) their potential to facilitate endosomal escape and 2) suitable binding capability to release cargoes (28, 29) (Fig. 2*H*). Furthermore, we assessed how the branched degree of tails on lipidoids, referring to the length of the branched structure, directed siRNA delivery. Lipidoids with a branched degree of 3 exhibited the highest siRNA delivery, up to 25%, compared to other branched degrees (Fig. 2*I*), consistent with previous studies (25, 30). We then investigated whether different formulation parameters affected siRNA delivery in vitro. Formulation parameters containing DOPE and/or C14PEG2K displayed better knockdown capability than formulations using DSPC and/or DMG-PEG2K, which may result from the relative lower encapsulation efficacy of DSPC-based formulations (*SI Appendix*, Table S2). Within this library, branched 4-O10b1 lipidoid under the formulation parameter A, demonstrating the highest GFP silencing efficacy, was further purified and selected as the top performer for the following in vitro and in vivo studies (*SI Appendix*, Fig. S5). We further explored the median effective dose (ED_{50}) of 4-O10b1 LNP for GFP gene silencing in vitro through flow cytometry (~7.2 nM, *SI Appendix*, Fig. S9). To demonstrate the enhanced delivery efficacy and endosomal escape performance attributable to branched structures, a similar lipioid with linear structured tails was synthesized (4-O10, *SI Appendix*, Fig. S6) to assess as a nonbranched but otherwise nearly identical control. We hypothesized that the branched structure could increase the distance between tails to form a more cone-shaped ion pair with the anionic membrane phospholipid to enhance endosome disruption (31). To verify this, the packing parameter (*P*) of branched and linear lipidoids was calculated from molecular dynamics simulation (Fig. 2 *K* and *I*). Our results showed that the *P* value of 4-O10b1 (P = 2.60) was larger than that of 4-O10 (P = 2.17), indicating that 4-O10b1 is more likely to induce the rupture of the endosomal membrane. We next evaluated the membrane-disruptive activities of these lipidoids using hemolysis assay (Fig. 2*M* and *SI Appendix*, Fig. S10). 4-O10b1 LNP exhibited stronger hemolysis than 4-O10 LNP, especially at acidic pH. These results collectively highlight the utility of branched LNP formulations for enhancing siRNA delivery efficacy in vitro.

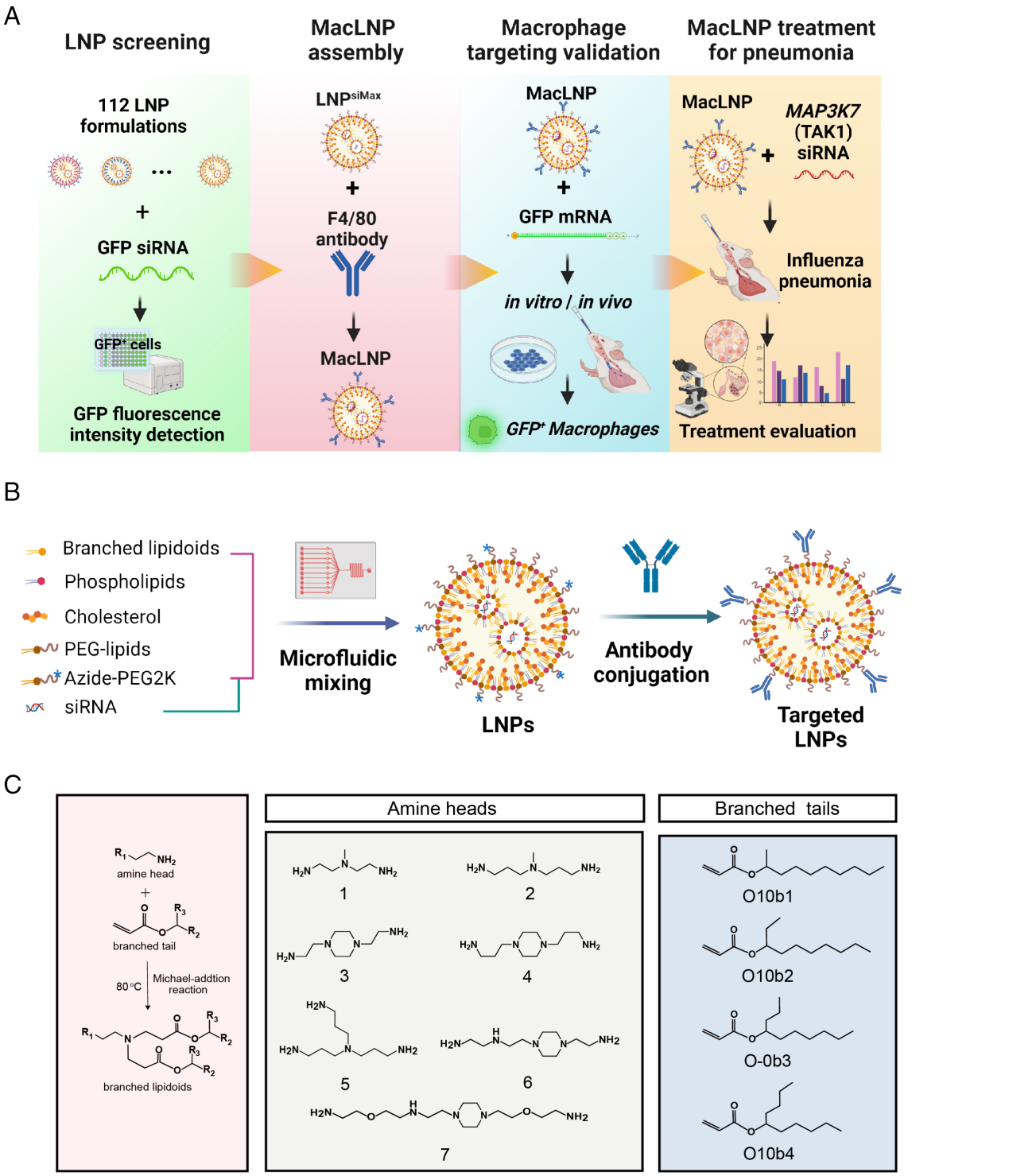

Fig. 1. Design of LNP formulations. (*A*) Study synopsis: LNP formulation design, screening, MacLNP assembly and validation, and in vivo application. (*B*) An antibody-modification strategy was utilized to conjugate antibody onto branched LNP surfaces for active targeting. Branched LNPs were formulated with branched lipidoids, phospholipids, cholesterol, PEG-lipids, and azide-PEG2K. The resulting branched LNPs were further incubated with DBCO-activated antibody for targeted LNPs formulation. (*C*) A list of seven amine cores and four branched tails was used for combinatorial design and synthesis of 28 branched lipidoids through a Michael-addition reaction.

Enhanced Macrophage Delivery Efficiency via F4/80 Antibody-conjugated Branched LNPs. Incorporation of ligands into LNP formulations, including small molecules (32, 33), peptides (34), and antibodies (35, 36), represents a useful strategy to deliver genetic drugs into specific cells and tissues of interest (37). Among them, antibody-conjugating strategies have already been demonstrated to selectively target cell types with minimum side effects in various therapeutic applications (35, 36, 38). Macrophages are dynamic cells involved in innate immunity, tissue development, homeostasis, and repair, and are widely utilized in in vitro research platforms (2, 39, 40). However, they are also challenging targets for transfection (41). To achieve effective targeted delivery to macrophages, we employed an antibody conjugation strategy as previously described (42) In short, a strain-promoted alkyne azide cycloaddition (SPAAC)

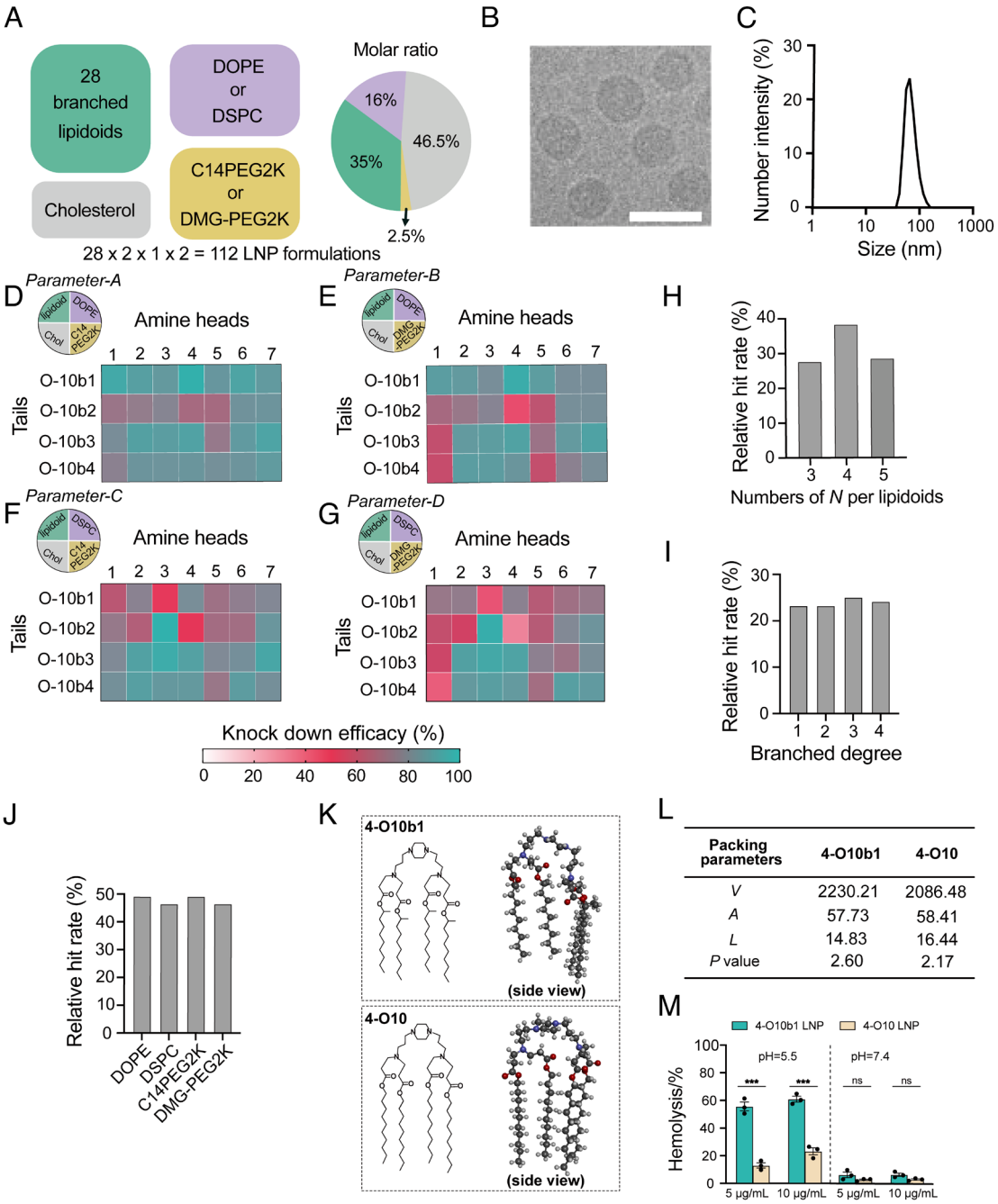

Fig. 2. In vitro screening of branched LNPs for siRNA delivery. (*A*) Branched LNPs were formulated through pipette mixing of an ethanol phase containing branched lipidoids (35%, molar ratio), phospholipids (DOPE or DSPC, 16%, molar ratio), cholesterol (46.5%, molar ratio), and PEG-lipids (C14PEG2K or DMG-PEG2K, 2.5%, molar ratio) and an aqueous phase containing siRNA. (*B*) A representative cryogenic transmission electron microscopy (cyro-TEM) image of branched LNP formulated by microfluidic mixing. (Scale bar: 100 nm.) (*C*) Hydrodynamic size of the representative branched LNP in *B*. (*D*–*G*) Heat maps of GFP knockdown following treatment of HepG2-GFP cells with branched LNPs delivering siGFP at a concentration of 50 nM formulated under different parameters (n ≥ 3 replicates). (*D*) LNPs were formulated under parameter A with ethanol phase containing branched lipidoods, DOPE, cholesterol, and C14PEG2k. (*E*) LNPs were formulated under parameter B with ethanol phase containing branched lipidoids, DOPE, cholesterol, and DMG-PEG2K. (*F*) LNPs were formulated under parameter C with ethanol phase containing branched lipidoids, DSPC, cholesterol, and C14PEG2K. (*G*) LNPs were formulated under parameter D with ethanol phase containing branched lipidoids, DSPC, cholesterol, and DMG-PEG2K. (*H*–*J*) Structure–activity relationship (SAR) of branched LNPs for siRNA delivery. Relative hit rate (GFP silencing of >50%) was counted for GFP knockdown efficacy. (*H*) Relative hit rate of branched LNPs with different tertiary amine numbers per lipidoids. (*I*) Relative hit rate of branched LNPs with different branched degrees. (*J*) Relative hit rate of branched LNPs with different phospholipids and PEG-lipids. (*K*) Chemical structures of 4-O10b1 and 4-O10 lipidoids and their side view images generated from molecular dynamics simulations. (*L*) Critical packing parameters of 4-O10b1 and 4-O10 lipidoids calculated based on molecular dynamics simulations. (*M*) Hemolysis of LNPs with different dosages at pH 5.5 or 7.4. Red blood cells (RBCs) were incubated with LNPs at 37 °C for 1 h, and then, the supernatant was used to determine the adsorption at 540 nm. All data are presented as mean ± SEM (n = 3).

click chemistry method was utilized to integrate DBCO-activated F4/80 (a classical macrophage-specific marker in mice) antibody with as-prepared azide-4-O10b1-LNP (F4/80 LNP or MacLNP, Fig. 3*A*), with IgG2a-conjugated LNP (IgG LNP or Control LNP) as negative controls. The increased particle size and decreased zeta potential of LNPs after antibody conjugation demonstrated the successful antibody conjugation process (*SI Appendix*, Fig. S11). To assess the targeting specificity and transfection efficiency of MacLNP in vitro and in vivo, GFP mRNA-loaded LNPs, MacLNPs, and IgG LNPs were separately used for transfecting the murine macrophage

cell line RAW264.7 (Fig. 3*B*) and administered intranasally in vivo (Fig. 3*E*). We observed a significant transfection advantage of MacLNP compared to IgG LNP, both in vitro (Fig. 3 *C* and *D*) and in vivo (Fig. 3 *F* and *G*). No notable differences were observed between IgG LNP and untreated LNPs. In vivo GFP distribution indicates that MacLNP exhibits high specificity, targeting macrophages ($CD68^+$ and/or $F4/80^+$) effectively (Fig. 3*F* and *SI Appendix*, Fig. S12), with no observed targeting to other cell types (*SI Appendix*, Fig. S13). Notably, the lack of F4/80 antibody modification doesn't appear to impact macrophage targeting specificity but does result in a significant reduction in delivery/transfection efficiency (Fig. 3*F*). Meanwhile, reducing MacLNP GFP dosage to 0.75 mg/kg revealed significant targeting efficiency even at lower doses (*SI Appendix*, Fig. S14). Furthermore, to investigate the in vivo duration of MacLNP-mediated RNA delivery, we surveyed GFP-expressing cells after MacLNP administration for 2 to 7 d. Our data indicated a significant reduction in GFP+ macrophages on day 3, with almost no GFP+ cells observed by day 7 (*SI Appendix*, Fig. S15). As SM-102 LNP is a crucial component in the FDA-approved mRNA-based COVID-19 vaccine, we next compared the delivery efficacy of MacLNP (4-10b1) with MacLNP (SM-102). We observed that when delivering GFP mRNA, SM102 F4/80 LNP (MacLNP) demonstrated in vivo targeting specificity and transfection efficiency comparable to the MacLNP used in this study, namely 4-10b1 MacLNP. Intriguingly, SM102 MacLNP exhibited very low GFP mRNA transfection efficiency in RAW264.7 cells (*SI Appendix*, Fig. S16). This indicated that the inconsistency in transfection between in vivo and in vitro settings may be due to differences in the microenvironment. Taken together, this suggests that the F4/80 antibody conjugation likely enhances the attachment/enrichment of LNPs on the macrophage surface, thus increasing the delivery efficiency.

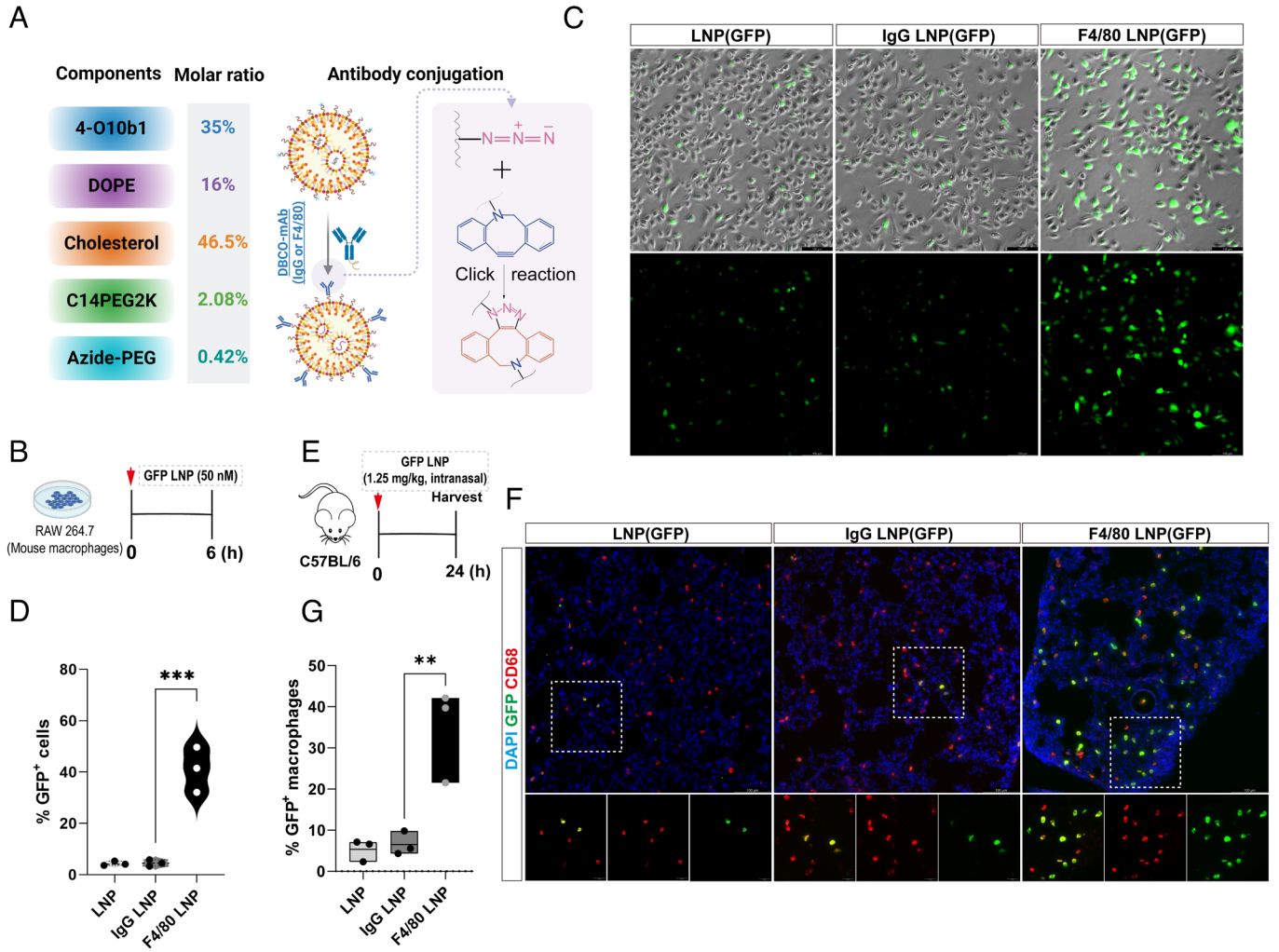

Fig. 3. Validation of F4/80-conjugated LNP for macrophage delivery. (*A*) Schematic representation of the antibody-conjugated branched LNPs formulation. Azide LNP was formulated by microfluidics mixing of an ethanol phase containing 4-O10b1 lipidoid (35%, molar ratio), DOPE (16%, molar ratio), cholesterol (46.5%, molar ratio), C14PEG2K (2%, molar ratio), and azide-PEG (0.5%, molar ratio) with an aqueous phase containing siRNA. Subsequently, DBCO-activated monoclonal antibody (mAb) was incubated with the above LNP solution for clickable conjugation. (*B–D*) (*B*) RAW264.7 cells were resuspended in 2 mL of Opi-MEM culture medium to obtain a single-cell suspension. These cells then mixed with LNP containing GFP mRNA (50 nM) as follows: LNP (no antibody conjugation), IgG LNP, and F4/80 LNP. The LNP-cell mixtures were then evenly distributed into a six-well plate. After 6 h, fluorescence microscopy was used to evaluate GFP expression. (*C*) Representative images of GFP expression from each group under the microscope. (Scale bar: 100 μm.) (*D*) Quantification of GFP cells, data are presented as means ± SEM (n = 3), calculated using one-way ANOVA, followed by Dunnett's multiple comparison test, $^{***}P < 0.001$. (*E–G*) (*E*) C57BL/6 mice were intranasally administered GFP-encapsulated LNPs, including LNP (without antibody conjugation), IgG LNP, and F4/80 LNP. Dexamethasone (DEX) was injected intraperitoneally (2 mg/kg; i.p.) 1 h prior to LNPs injection in all mice. Samples were collected 24 h later to observe GFP expression. (*F*) Representative images of macrophages ($CD68^+$) expressing GFP from each group. (Scale bar: 100 μm.) (*G*) Quantification of GFP^+ macrophages, data are presented as means ± SEM (n = 3), calculated using one-way ANOVA, followed by Dunnett's multiple comparison test, $^{**}P < 0.01$.

MacLNP-mediated Targeted Knockdown of TAK1 Inhibits the Release of Proinflammatory Cytokines in RAW264.7 Cells. Macrophages release numerous proinflammatory cytokines while recognizing and eliminating bacterial and viral pathogens, but excessive cytokine production can exacerbate tissue damage (4, 43). M1-like macrophages, a subtype activated by microbial products or proinflammatory signals, are crucial for the immune system's inflammatory response. They release cytokines like IL-1β, IL-6, and TNF-α, playing a role in host defense and pathogen removal. Prolonged M1-like activation, though, may lead to chronic inflammation and tissue damage (44). Adjusting proinflammatory cytokine release to control inflammation holds promise for treating diverse diseases characterized by overexuberant inflammation. NF-κB is a critical signaling pathway that triggers the classical activation (M1-like) of macrophages (45). Upon stimulation, the NF-κB subunit p65 undergoes phosphorylation and is subsequently translocated into the nucleus, initiating downstream effector mechanisms and inducing the production of proinflammatory mediators including the aforementioned cytokines (46). TAK1 activates the NF-κB pathway, playing a vital role in the inflammatory process, and holds potential as a therapeutic target for inflammatory disorders (21). We therefore investigated whether blocking TAK1 using MacLNP for siRNA delivery could reduce NF-κB activation and consequently decrease the release of proinflammatory cytokines. After in vitro treatment with MacLNP containing TAK1 siRNA (si-TAK1), we noted a significant decrease in TAK1 expression (Fig. 4*A*), indicating the feasibility of the MacLNP approach. Next, we explored whether reducing TAK1 expression using MacLNP/siTAK1 affects the activation of NF-κB and the release of proinflammatory cytokines. As shown in Fig. 4*B*, RAW264.7 cells transfected with si-TAK1 or control siRNA (si-NC) were exposed to the viral RNA mimic and TLR3 agonist Poly(I:C) for 1 or 24 h. Poly(I:C) significantly promoted NF-κB phosphorylation, as expected. However, si-TAK1 notably suppressed Poly(I:C)-induced NF-κB phosphorylation levels (Fig. 4 *C* and *D*). Similarly, si-TAK1 inhibited the levels of proinflammatory cytokines IL-1β, IL-6, and TNF-α induced by Poly(I:C) (Fig. 4 *E*–*G*). These results suggest that MacLNP-mediated si-TAK1 effectively mitigate macrophage inflammatory responses associated with the classical "M1" phenotype (Fig. 4*H*).

MacLNP-mediated Targeted Knockdown of TAK1 in Macrophages Alleviates Viral Pneumonia. Macrophages, the most abundant resident immune cell in the lung, represent the first line of defense, recognizing pathogens, releasing cytokines, aiding tissue repair, and playing a vital role in innate immunity (47). Attenuating the release of proinflammatory cytokines, especially in proinflammatory (M1-like) macrophages, can potentially reduce local inflammatory responses, promoting tissue repair (2, 10, 39). Based on our findings above demonstrating that MacLNP effectively enhances targeted delivery efficiency to macrophages can be employed to reduce TAK1 expression and subsequent proinflammatory cytokine release, we investigated whether in vivo MacLNP delivery of si-TAK1 could alleviate morbidity resulting from viral pneumonia. C57BL/6 mice were treated with equal volume of PBS, control siRNA(si-NC), or TAK1 siRNA (si-TAK1) MacLNP (1.25 mg/kg, 40 μL) on days 15 and 20 postinfection intranasally and samples were collected at the indicated time points. Given that LNPs may themselves trigger an immediate immune response, potentially exacerbating inflammation in the treatment of inflammatory diseases, we employed pretreatment with dexamethasone (DEX) which has been demonstrated to effectively manage LNP-induced inflammation (48, 49). Indeed, mice not pretreated with DEX exhibited a strong trend toward increased inflammation upon intranasal administration of MacLNP GFP, while DEX (2 mg/kg; i.p.) treatment alleviated this condition (*SI Appendix*, Fig. S17). Additionally, to clarify the potential immunogenic side effects of our MacLNP, we used standard SM-102 LNP as a control. Our results confirm that MacLNP and SM-102 exhibit similar immunogenicity. This was evidenced by the assessment of the total immune cell population ($CD45^+$) in the lungs and the levels of inflammatory cytokines in BALF, including TNF-α, IL-6, MCP-1/CCL-2, and IFN-γ. Furthermore, treatment of RAW264.7 cells with MacLNP or SM-102 LNP resulted in similar levels of TNF-α, IL-6, IL-1β, MCP-1/CCL-2, and IL-12 in the cell supernatant. Notably, both types of LNPs demonstrated some proinflammatory effects as expected, but pretreatment with DEX lessened this trend (*SI Appendix*, Fig. S18). Thus, DEX was injected intraperitoneally (2 mg/kg; i.p.) 1 h prior to MacLNPs injection in all mice (Fig. 5*A*). We observed that MacLNP/si-TAK1 treatment resulted in less local inflammation during viral injury, as evidenced by decreased levels of total protein (Fig. 5*B*), myeloperoxidase (MPO) activity (Fig. 5*C*), and proinflammatory cytokines TNF-α, IL-1β and IL-6 (Fig. 5 *D*–*F*) present in the bronchoalveolar lavage fluid (BALF) in comparison to mice treated with MacLNP/si-NC control. Histologic analysis of the lungs supported these findings and revealed reduced injury following MacLNP/si-TAK1 treatment, as assessed through an unbiased computational imaging method (50) (Fig. 5 *G* and *H*). However, we also noticed a slight increase in histopathology in mice treated with si-NC LNPs compared to mice treated with PBS only, even though all animals were pretreated with DEX. In addition, while targeting TAK1 has displayed promising results in reducing fibrosis (21), we did not observe a significant reduction in lung fibrosis resulting from influenza injury through MacLNP-mediated delivery of TAK siRNA (*SI Appendix*, Fig. S19). This may be attributed to the targeting of different cell types and/or different models of fibrosis. These observations suggest that LNP targeting of macrophages to reduce TAK1 levels offers protection against severe influenza pneumonia, partially by diminishing local inflammation, but also reinforces that LNP delivery in and of itself can promote some degree of inflammation.

Discussion

Here, we present an LNP delivery strategy targeting alveolar macrophages. Using MacLNP-mediated delivery of TAK siRNA during lung injury effectively reduces the inflammation caused by macrophage-released proinflammatory cytokines, thereby ameliorating lung injury. This provides a broad avenue and strategy for the clinical treatment of inflammatory diseases.

Macrophages, originating from proliferation of resident alveolar macrophages or from precursor monocytes through tissue-specific differentiation, migrate to infection or injury sites and produce inflammatory signals like chemokines, cytokines, and other cascading products. They can adopt a spectrum of phenotypes bookended by two major states: M1, which is a proinflammatory phenotype, and M2, which is anti-inflammatory and prorepairative. M1 macrophages release proinflammatory cytokines, such as TNF-α, IL-6, and IL-1β, and boost inflammation. M2 macrophages, on the other hand, express IL-10 and IL-1RA, aiding in pathogen clearance, dampening inflammation, promoting tissue repair (1, 39, 44, 51, 52). The balance between these two macrophage phenotypes is crucial in governing the body's inflammatory response, influencing the onset, development, and resolution

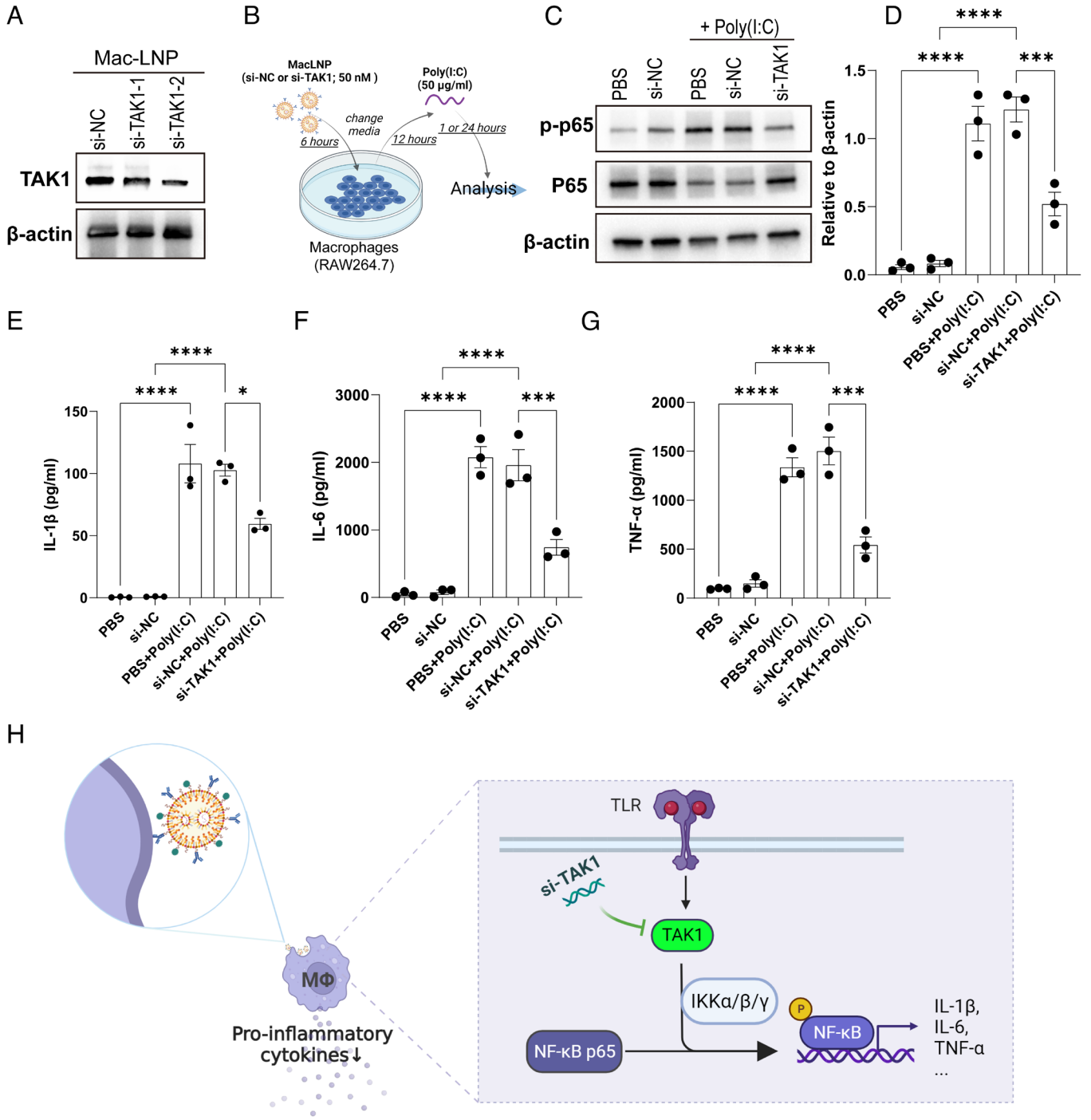

Fig. 4. MacLNP delivery of TAK1 siRNA inhibits the release of proinflammatory cytokines in RAW264.7 cells. (*A*) RAW264.7 cells were transfected with siRNAs [50 nM, control siRNA (si-NC) and TAK1 siRNA (si-TAK1)] encapsulated in F4/80 LNP (MacLNP). TAK1 expression was analyzed using western blotting at 24 h posttransfection. (*B–G*) (*B*) After transfection of RAW264.7 cells with MacLNP encapsulating siRNAs [50 nM; control siRNA (si-NC) and TAK1 siRNA (si-TAK1)], the cells were switched to complete culture medium after 6 h. Subsequently, they were cultured for an additional 12 h and then exposed to Poly(I:C) (50 μg/mL) for 1 h (for western blot analysis) or 24 h (supernatant collection for ELISA). (*C*) Western blot analysis was conducted to assess the phosphorylation levels of NF-κB p65. (*D*) Quantitative analysis was performed to measure the phosphorylation levels of NF-κB p65 relative to β-actin. ELISA was used to detect the levels of proinflammatory cytokines IL-1β (*E*), IL-6 (*F*), and TNF-α (*G*) in the supernatant. Data are presented as means ± SEM (n = 3), calculated using one-way ANOVA, followed by Dunnett's multiple comparison test, ***$P < 0.001$, ****$P < 0.0001$. (*H*) The diagram shows how MacLNP delivers *TAK1* (*MAP3K*) siRNA to reduce proinflammatory cytokine release from macrophages.

of inflammatory conditions (39). As such, macrophages hold a pivotal role in preserving homeostasis and modulating the inflammatory responses when needed. Thus, considerable emphasis has been laid upon targeted therapies against them to treat inflammatory diseases (3, 9, 10). A widely employed strategy involves aiding these cells in engulfing micro- or nanoscale delivery vehicles loaded with therapeutic agents (9). This passive targeting leverages the mounting immune response, directing the delivery vehicle to the inflammation site. Alternatively, the delivery vehicle's surface can be decorated with a ligand that specifically interacts with the target receptors on macrophages (42). In this study, we initially screened for the most effective LNP formulation for gene knockdown using GFP siRNA. Subsequently, we employed the antibody-LNP conjugation technique to create LNPs that can specifically bind the

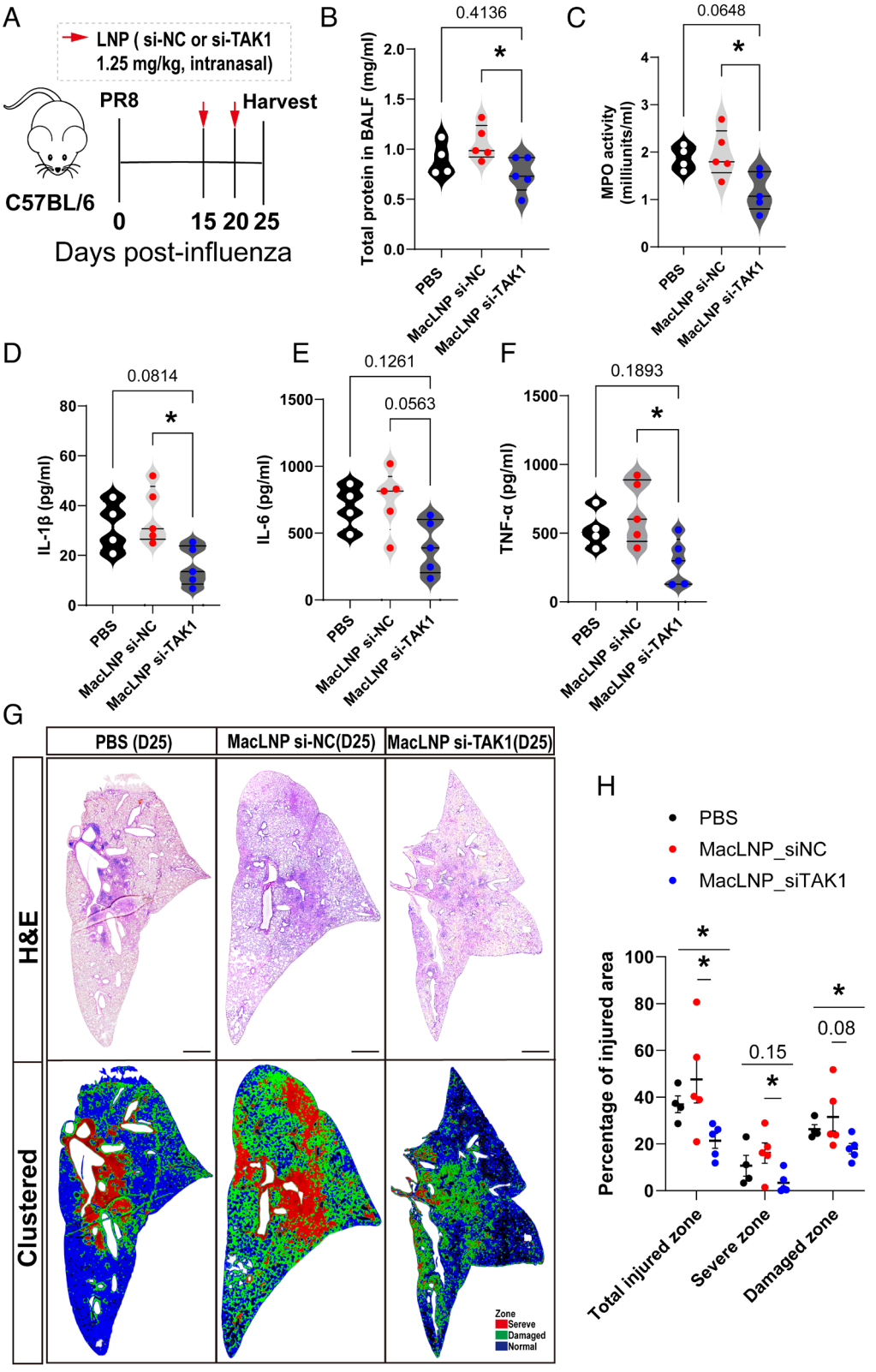

Fig. 5. MacLNP delivery of TAK siRNA for the treatment of viral lung injury. (*A*) Timeline for MacLNP administration and sampling. C57BL/6 mice were treated with PBS or MacLNPs encapsulating control siRNA (si-NC) or TAK1 siRNA (si-TAK1) (1.25 mg/kg, intranasal) on days 15 and 20 postinfection, and samples were collected on day 25 postinfection. Dexamethasone-21-Phosphate (DEX) was injected intraperitoneally (i.p. 2 mg/kg) into the mice 1 h prior to PBS/LNP administration in all mice. (*B* and *C*) Total protein (*B*) and MPO activity (*C*) were quantified in BALF collected from mice which received treatment as described in *A* harvested on day 25 after infection. Data are represented as mean ± SEM (n = 4 to 5 mice/group), calculated using one-way ANOVA, followed by Dunnett's multiple comparison test, $*P < 0.05$. (*D–F*) The concentration of proinflammatory cytokines, IL-1β (*D*), IL-6 (*E*), and TNF-α (*F*) in BALF was measured by ELISA from mice which received treatment as described in *A* and harvested on day 25 after infection. Data are represented as mean ± SEM (n = 4 to 5 mice/group), calculated using one-way ANOVA, followed by Dunnett's multiple comparison test, $*P < 0.05$. (*G* and *H*) (*G*) *Upper*: Tile scan images of H&E stain; *Lower*: clustered injury zone maps produced from upper H&E images. (Scale bars: 1 mm.) (*H*) Quantification of relative area in different injury zones in *G*. Data are represented as mean ± SEM (n = 4 to 5 mice/group), calculated using an unpaired two-tailed *t* test, $*P < 0.05$.

macrophage surface antigen F4/80, enhancing macrophage delivery efficiency. While our data validated the significantly improved delivery efficiency of F4/80 antibody-conjugated LNPs, in vivo results indicated that almost all GFP LNPs delivered through nasal administration were transduced only into macrophages even without antibody incorporation. (Fig. 3*F*). This suggests that LNPs introduced into the lung through inhalation are initially subjected to phagocytosis/clearance by macrophages. While this characteristic prevents off-target effects in therapies aimed at macrophages, it also presents challenges in developing delivery tools targeting other cell types within the lung, especially for nasal administration of nanovaccines development or gene correction of airway or alveolar epithelial cells. Although our data demonstrate that the F4/80-LNP strategy effectively targets lung macrophages, this occurs in the context of in situ delivery of LNPs rather than systemic administration, such as intravenous injection. It is therefore uncertain whether this strategy would be effective via systemic administration. Additionally, since dendritic cells (DCs) also express F4/80, despite our data showing that GFP-expressing cells are $CD68^+F480^+SiglecF^+$ alveolar macrophages (*SI Appendix*, Fig. S13), we cannot rule out the possibility of some limited targeting of DCs. TAK1 is crucial for DC survival and development (53), and thus, the F4/80 antibody modification strategy may affect the development and survival of a small subset of DCs. Therefore, developing more specific antibodies is one of the key challenges in the LNP antibody conjugation strategy for in vivo targeting.

Extensive research has been conducted on lipid-based nanoparticles as delivery platforms for nucleic acid therapy targeting various diseases (3, 8, 9, 16, 29, 36). LNPs are gaining prominence as the leading nonviral nanocarrier for in vivo gene editing/therapy. They typically exhibit minimal cytotoxicity and immunogenicity and are relatively straightforward to synthesize and produce (54), and more than ten pharmaceuticals employing LNPs for drug or mRNA delivery are US Food and Drug Administration (FDA) approved, including Pfizer/BioNTech's and Moderna's COVID-19 mRNA vaccines (55–57). Encouragingly, LNPs have been utilized to generate transient CAR-T cells in vivo for the treatment of cardiac fibrosis (35). Although LNPs have demonstrated promising results as delivery tools in mouse models, they still face challenges when employed as therapeutic agents. First and foremost is the issue of targeting specific tissues or cells with LNP delivery. While considerable progress has been made to achieve targeted delivery to various cell types within different organs such as the liver (58), spleen (58), and lungs (14, 58, 59), research on tissue/cell targeting in larger animals and even primates remains limited. Second, the route of LNP administration is crucial. Systemic administration, such as intravenous delivery, is the primary method currently used, but it also carries higher immune risks. Therefore, local administration may be relatively safer. We observed that nasal administration effectively reaches the lungs, yet it poses the challenge of uneven distribution of LNPs across the tissue. Nebulized LNPs seem promising (14), but they might come with higher costs. Last, LNPs are foreign substances that can trigger an immediate immune response from the body's immune system, posing a risk of exacerbating inflammation when used to treat inflammatory diseases (30, 48, 49). Some studies have shown that using dexamethasone before LNP treatment can effectively control the immediate inflammatory reaction caused by LNPs (48, 49). In our study, before treating mice with MacLNP to deliver TAK1 siRNA for viral lung injury, all mice were pretreated with dexamethasone, and we did not observe significant worsening of inflammation during the experiment. That being said, mice treated with siLNP trended toward worsened histopathology compared to mice treated only with saline, though this was effectively overcome in the siTAK1 treatment group, reinforcing the care that needs to be taken when considering delivery LNP therapeutics. Furthermore, we believe that the timing of LNP administration is critical. Therefore, in future applications, LNP-mediated gene therapy may need to be combined with other approaches for effective disease treatment.

In theory, siRNA can specifically halt the production of disease-related proteins. However, putting siRNA into clinical use has presented major challenges. These encompass safeguarding siRNA from degradation in bodily fluids, specific delivery to target tissues, and transporting it to the target cell's cytoplasm. LNPs are thus promising vehicles to overcome these siRNA delivery challenges. LNPs containing improved ionizable cationic lipids have shown impressive in vivo effects, silencing liver target genes at incredibly low siRNA doses (as little as 0.005 mg/kg body weight) via intravenous injection in rodents (26). These systems are relatively safe and hold promise for clinical use. TAK1 is recognized as a stimulating kinase for the IκB kinase (IKK) complex, which includes IKKα, IKKβ, and NF-κB essential modulator (NEMO). This activation occurs by associating with TNF receptor-associated factor 2 (TRAF2) in the TNF-α pathway and TRAF6 in the IL-1–TLR pathway (20). TAK1 is therefore of great interest as a major target kinase promoting inflammatory disorders (20, 21). Indeed, TAK1 blockade has been shown to profoundly suppress inflammation and fibrosis (21, 60). By employing MacLNP to deliver TAK1 siRNA, we observed a reduction in inflammation both in vitro and in vivo, which was evidenced by the decrease in levels of proinflammatory cytokines. While specific disease states will be best served by discrete siRNA targets, we believe that our work here targeting TAK1 with macrophage-targeted LNPs represents very strong proof of principle for future development of macrophage-targeted therapeutics.

In sum, this study significantly enhanced the targeted delivery efficiency to macrophages using our newly designed MacLNP. Through in vivo targeted siRNA delivery, it effectively ameliorated viral lung injury, offering a therapeutic avenue for clinical treatment of inflammatory diseases and facilitating approaches to future macrophage-targeted therapies.

Materials and Methods

Detailed materials and methods are provided in *SI Appendix, Materials and Methods*, including all materials and instruments, chemical synthesis and characterization of LNPs, and all in vitro and in vivo biological assays. All animal experiments were carried out under the guidelines set by the University of Pennsylvania's Institutional Animal Care and Use Committees and followed all NIH Office of Laboratory Animal Welfare regulations. Key techniques and protocols used in this manuscript are summarized below, with fully detailed descriptions present in *SI Appendix*.

Cell Culture. HepG2-GFP cells (John M. Maris Laboratory) were cultured in Dulbecco's Modified Eagle Medium (DMEM, Gibco) supplemented with 10% fetal bovine serum (FBS, Sigma-Aldrich) and 1% penicillin–streptomycin (P/S, Gibco). RAW264.7 (ATCC TIB-71™) were cultured in RPMI 1640 media with GlutaMAX supplement added, containing 10% cosmic calf serum (CC; HyClone, #SH3008704) and 1% penicillin/streptomycin (P/S; Gibco, #15140122).

Animal Studies. Six- to 8-wk old C57BL/6J mice of both sexes were administered influenza virus A/H1N1/PR/8 at 50 to 75 TCID50 units. Mice were weighed regularly and killed at the indicated time points for tissue harvest. LNP formulations were delivered to anesthetized mice via intranasal inhalation.

Synthesis of Branched Ionizable Lipids. Branched ionizable lipids were synthesized by Michael addition reaction between seven different amine cores and four different branched tails. Taking synthesis of 4-O10b1 as an example,

core 1 (117.2 mg, 1 mmol, 1 equiv) and O10b1 (1.02 g, 4.8 mmol, 4.8 equiv) were dissolved in ethanol and added in a glass vial equipped with a stir bar. The reaction was stirred at 80 °C for 2 d. The crude product was afforded by removing the solvents and was used to screen the library for siGFP delivery in vitro without further purification.

Data, Materials, and Software Availability. All study data are included in the article and/or *SI Appendix*.

ACKNOWLEDGMENTS. We thank all Vaughan Lab members for helpful discussions and suggestions and BioRender for providing a platform to create the cartoons and schematics used in figures throughout this report. This work was supported by the following: NIH R01HL153539 (A.E.V.); NIH 01HL164350 (A.E.V.); Margaret Q. Landenberger Foundation (A.E.V.); NIH Director's New Innovator Award DP2 TR002776 (M.J.M.); Burroughs Wellcome Fund Career Award at the Scientific Interface (M.J.M.); and NSF CAREER award CBET-2145491 (M.J.M.).

Author affiliations: [a]Department of Biomedical Sciences, School of Veterinary Medicine, University of Pennsylvania, Philadelphia, PA 19104; [b]Institute for Regenerative Medicine, University of Pennsylvania, Philadelphia, PA 19104; [c]Penn-Children's Hospital of Philadelphia Lung Biology Institute, University of Pennsylvania, Philadelphia, PA 19104; [d]Department of Bioengineering, University of Pennsylvania, Philadelphia, PA 19104; [e]Penn Institute for RNA Innovation, Perelman School of Medicine, University of Pennsylvania, Philadelphia, PA 19104; [f]Abramson Cancer Center, Perelman School of Medicine, University of Pennsylvania, Philadelphia, PA 19104; [g]Institute for Immunology, Perelman School of Medicine, University of Pennsylvania, Philadelphia, PA 19104; and [h]Cardiovascular Institute, Perelman School of Medicine, University of Pennsylvania, Philadelphia, PA 19014

1. T. A. Wynn, K. M. Vannella, Macrophages in tissue repair, regeneration, and fibrosis. *Immunity* **44**, 450–462 (2016).
2. S. Watanabe, M. Alexander, A. V. Misharin, G. R. S. Budinger, The role of macrophages in the resolution of inflammation. *J. Clin. Invest.* **129**, 2619–2628 (2019).
3. W. Chen *et al.*, Macrophage-targeted nanomedicine for the diagnosis and treatment of atherosclerosis. *Nat. Rev. Cardiol.* **19**, 228–249 (2022).
4. D. McGonagle, K. Sharif, A. O'Regan, C. Bridgewood, The role of cytokines including interleukin-6 in COVID-19 induced Pneumonia and Macrophage Activation Syndrome-Like Disease. *Autoimmun Rev.* **19**, 102537 (2020).
5. T. Suzuki *et al.*, Increased pulmonary GM-CSF causes alveolar macrophage accumulation mechanistic implications for desquamative interstitial pneumonitis. *Am. J. Resp. Cell Mol.* **62**, 87–94 (2020).
6. A. Akinc *et al.*, A combinatorial library of lipid-like materials for delivery of RNAi therapeutics. *Nat. Biotechnol.* **26**, 561–569 (2008).
7. J. E. Dahlman *et al.*, In vivo endothelial siRNA delivery using polymeric nanoparticles with low molecular weight. *Nat. Nanotechnol.* **9**, 648–655 (2014).
8. X. C. Hou, T. Zaks, R. Langer, Y. Z. Dong, Lipid nanoparticles for mRNA delivery. *Nat. Rev. Mater* **6**, 1078–1094 (2021).
9. A. Singh, M. Talekar, A. Raikar, M. Amiji, Macrophage-targeted delivery systems for nucleic acid therapy of inflammatory diseases. *J. Control Release* **190**, 515–530 (2014).
10. A. Costa, B. Sarmento, V. Seabra, Targeted drug delivery systems for lung macrophages. *Curr. Drug Targets* **16**, 1565–1581 (2015).
11. J. R. McCarthy, F. A. Jaffer, R. Weissleder, A macrophage-targeted theranostic nanoparticle for biomedical applications. *Small* **2**, 983–987 (2006).
12. A. Radmand *et al.*, The transcriptional response to lung-targeting lipid nanoparticles in vivo. *Nano Lett.* **23**, 993–1002 (2023).
13. M. Qiu *et al.*, Lung-selective mRNA delivery of synthetic lipid nanoparticles for the treatment of pulmonary lymphangioleiomyomatosis. *Proc. Natl. Acad. Sci. U.S.A.* **119**, e2116271119 (2022).
14. M. P. Lokugamage *et al.*, Optimization of lipid nanoparticles for the delivery of nebulized therapeutic mRNA to the lungs. *Nat. Biomed Eng.* **5**, 1059–1068 (2021).
15. Q. Cheng *et al.*, Selective organ targeting (SORT) nanoparticles for tissue-specific mRNA delivery and CRISPR-Cas gene editing. *Nat. Nanotechnol.* **15**, 313–320 (2020).
16. J. M. McLendon *et al.*, Lipid nanoparticle delivery of a microRNA-145 inhibitor improves experimental pulmonary hypertension. *J. Control Release* **210**, 67–75 (2015).
17. A. K. K. Leung, Y. Y. C. Tam, P. R. Cullis, Lipid nanoparticles for short interfering RNA delivery. *Adv. Genet.* **88**, 71–110 (2014).
18. O. Taratula, A. Kuzmov, M. Shah, O. B. Garbuzenko, T. Minko, Nanostructured lipid carriers as multifunctional nanomedicine platform for pulmonary co-delivery of anticancer drugs and siRNA. *J. Control Release* **171**, 349–357 (2013).
19. M. Zoulikha *et al.*, Pulmonary delivery of siRNA against acute lung injury/acute respiratory distress syndrome. *Acta Pharm. Sin B* **12**, 600–620 (2022).
20. H. Sakurai, Targeting of TAK1 in inflammatory disorders and cancer. *Trends Pharmacol. Sci.* **33**, 522–530 (2012).
21. J. Li *et al.*, TAK1 inhibition attenuates both inflammation and fibrosis in experimental pneumoconiosis. *Cell Discov.* **3**, 17023 (2017).
22. K. A. Hajj *et al.*, Branched-tail lipid nanoparticles potently deliver mRNA in vivo due to enhanced ionization at endosomal pH. *Small* **15**, e1805097 (2019).
23. K. A. Hajj *et al.*, A potent branched-tail lipid nanoparticle enables multiplexed mRNA delivery and gene editing in vivo. *Nano Lett.* **20**, 5167–5175 (2020).
24. G. Sahay, Y. Eygeris, M. Gupta, J. Kim, Chemistry of lipid nanoparticles for RNA delivery published as part of the accounts of chemical research special issue "mRNA Therapeutics". *Accounts Chem. Res.* **55**, 2–12 (2022).
25. K. Hashiba *et al.*, Branching ionizable lipids can enhance the stability, fusogenicity, and functional delivery of mRNA. *Small Sci.* **3**, 2200071 (2023).
26. S. C. Semple *et al.*, Rational design of cationic lipids for siRNA delivery. *Nat. Biotechnol.* **28**, 172–176 (2010).
27. S. J. Shepherd *et al.*, Scalable mRNA and siRNA lipid nanoparticle production using a parallelized microfluidic device. *Nano Lett.* **21**, 5671–5680 (2021).
28. K. A. Whitehead *et al.*, Degradable lipid nanoparticles with predictable in vivo siRNA delivery activity. *Nat. Commun.* **5**, 4277 (2014).
29. S. G. Qin *et al.*, mRNA-based therapeutics: Powerful and versatile tools to combat diseases. *Signal Transduct. Target. Ther.* **7**, 166 (2022).
30. Y. H. Zhang *et al.*, Enhanced immunogenicity induced by mRNA vaccines with various lipid nanoparticles as carriers for SARS-CoV-2 infection. *J. Mater Chem. B* **11**, 7454–7465 (2023), 10.1039/d3tb00303e.
31. X. X. Han *et al.*, An ionizable lipid toolbox for RNA delivery. *Nat. Commun.* **12**, 7233 (2021).
32. L. L. Xue *et al.*, Rational design of bisphosphonate lipid-like materials for mRNA delivery to the bone microenvironment. *J. Am. Chem. Soc.* **144**, 9926–9937 (2022).
33. M. Kim *et al.*, Engineered ionizable lipid nanoparticles for targeted delivery of RNA therapeutics into different types of cells in the liver. *Sci. Adv.* **7**, eabf4398 (2021).
34. J. Y. Qin *et al.*, RGD peptide-based lipids for targeted mRNA delivery and gene editing applications. *Rsc Adv.* **12**, 25397–25404 (2022).
35. J. G. Rurik *et al.*, CAR T cells produced in vivo to treat cardiac injury. *Science* **375**, 91 (2022).
36. R. Kedmi *et al.*, A modular platform for targeted RNAi therapeutics. *Nat. Nanotechnol.* **13**, 214 (2018).
37. S. A. Dilliard, D. J. Siegwart, Passive, active and endogenous organ-targeted lipid and polymer nanoparticles for delivery of genetic drugs. *Nat. Rev. Mater* **8**, 282–300 (2023).
38. E. Rohner, R. Yang, K. S. Foo, A. Goedel, K. R. Chien, Unlocking the promise of mRNA therapeutics. *Nat. Biotechnol.* **40**, 1586–1600 (2022).
39. G. Zhao *et al.*, Vascular endothelial-derived SPARCL1 exacerbates viral pneumonia through pro-inflammatory macrophage activation. BioRxiv [Preprint] (2023). https://doi.org/10.1101/2023.05.25.541966 (Accessed 8 January 2023).
40. T. Gauthier *et al.*, TGF-beta uncouples glycolysis and inflammation in macrophages and controls survival during sepsis. *Sci. Signal* **16**, eade0385 (2023).
41. S. X. M. Dong *et al.*, Transfection of hard-to-transfect primary human macrophages with Bax siRNA to reverse Resveratrol-induced apoptosis. *RNA Biol.* **17**, 755–764 (2020).
42. J. Nong *et al.*, Targeting lipid nanoparticles to the blood brain barrier to ameliorate acute ischemic stroke. BioRxiv [Preprint] (2023). https://doi.org/10.1101/2023.06.12.544645 (Accessed 8 January 2023).
43. M. Merad, J. C. Martin, Pathological inflammation in patients with COVID-19: A key role for monocytes and macrophages. *Nat. Rev. Immunol.* **20**, 355–362 (2020).
44. F. O. Martinez, S. Gordon, The M1 and M2 paradigm of macrophage activation: Time for reassessment. *F1000Prime Rep.* **6**, 13 (2014).
45. A. M. Timmer, V. Nizet, IKKbeta/NF-kappaB and the miscreant macrophage. *J. Exp. Med.* **205**, 1255–1259 (2008).
46. Q. Li, I. M. Verma, NF-kappaB regulation in the immune system. *Nat. Rev. Immunol.* **2**, 725–734 (2002).
47. S. Herold, K. Mayer, J. Lohmeyer, Acute lung injury: How macrophages orchestrate resolution of inflammation and tissue repair. *Front Immunol.* **2**, 65 (2011).
48. S. Ndeupen *et al.*, The mRNA-LNP platform's lipid nanoparticle component used in preclinical vaccine studies is highly inflammatory. *Iscience* **24**, 103479 (2021).
49. H. Parhiz *et al.*, Added to pre-existing inflammation, mRNA-lipid nanoparticles induce inflammation exacerbation (IE). *J. Control Release* **344**, 50–61 (2022).
50. D. C. Liberti *et al.*, Alveolar epithelial cell fate is maintained in a spatially restricted manner to promote lung regeneration after acute injury. *Cell Rep.* **35**, 109092 (2021).
51. A. Shapouri-Moghaddam *et al.*, Macrophage plasticity, polarization, and function in health and disease. *J. Cell Physiol.* **233**, 6425–6440 (2018).
52. P. J. Murray, Macrophage polarization. *Annu. Rev. Physiol.* **79**, 541–566 (2017).
53. Y. Wang *et al.*, Transforming growth factor beta-activated kinase 1 (TAK1)-dependent checkpoint in the survival of dendritic cells promotes immune homeostasis and function. *Proc. Natl. Acad. Sci. U.S.A.* **109**, E343–E352 (2012).
54. K. L. Swingle, A. G. Hamilton, M. J. Mitchell, Lipid nanoparticle-mediated delivery of mRNA therapeutics and vaccines. *Trends Mol. Med.* **27**, 616–617 (2021).
55. A. Akinc *et al.*, The Onpattro story and the clinical translation of nanomedicines containing nucleic acid-based drugs. *Nat. Nanotechnol.* **14**, 1084–1087 (2019).
56. X. Hou, T. Zaks, R. Langer, Y. Dong, Lipid nanoparticles for mRNA delivery. *Nat. Rev. Materials* **6**, 1078–1094 (2021).
57. X. Han *et al.*, An ionizable lipid toolbox for RNA delivery. *Nat. Commun.* **12**, 1–6 (2021).
58. Q. Cheng *et al.*, Selective organ targeting (SORT) nanoparticles for tissue-specific mRNA delivery and CRISPR-Cas gene editing. *Nat. Nanotechnol.* **15**, 313–320 (2020).
59. J. C. Kaczmarek *et al.*, Optimization of a degradable polymer-lipid nanoparticle for potent systemic delivery of mRNA to the lung endothelium and immune cells. *Nano Lett.* **18**, 6449–6454 (2018).
60. F. Y. Ma *et al.*, TGF-beta1-activated kinase-1 regulates inflammation and fibrosis in the obstructed kidney. *Am. J. Physiol. Renal Physiol.* **300**, F1410–F1421 (2011).